Mercury capture on a supported chlorocuprate(II) ionic liquid adsorbent studied using operando synchrotron X-ray absorption spectroscopy

Boada, R., Cibin, G., Coleman, F., Diaz-Moreno, S., Gianolio, D., Hardacre, C., Hayama, S., Holbrey, J. D., Ramli, R., Seddon, K. R., Srinivasan, G., & Swadzba-Kwasny, M. (2016). Mercury capture on a supported chlorocuprate(II) ionic liquid adsorbent studied using operando synchrotron X-ray absorption spectroscopy. *Dalton Transactions*, *45*(47), 18946-18953. https://doi.org/10.1039/c6dt03014a

Published in:
Dalton Transactions

Document Version:
Peer reviewed version

Mercury capture on a supported chlorocuprate(II) ionic liquid adsorbent studied using *operando* synchrotron X-ray absorption spectroscopy†

Roberto Boada,[a] Giannantonio Cibin,[a] Fergal Coleman,[b] Sofia Diaz-Moreno,[a] Diego Gianolio,[a] Christopher Hardacre,[b,c] Shusaku Hayama,[a] John D. Holbrey,[b*] Rafin Ramli,[b] Kenneth R. Seddon,[b] Geetha Srinivasan[b] and Małgorzata Swadźba-Kwaśny.[b]

Mercury scrubbing from gas streams using a supported 1-butyl-3-methylimidazolium chlorocuprate(II) ionic liquid ($[C_4mim]_2[Cu_2Cl_6]$) has been studied using *operando* EXAFS. Initial oxidative capture as $[HgCl_3]^-$ anions was confirmed, this was then followed by the unanticipated generation of mercury(I) chloride through comproportionation with additional mercury from the gas stream. Combining these two mechanisms leads to net one electron oxidative extraction of mercury from the gas with increased potential capacity and efficiency for supported ionic liquid mercury scrubbers.

Introduction

Mercury management, *i.e.* controlling its presence in gas and vapour streams, is of vital importance across a wide range of industrial sectors, including power generation (oil and gas industries, coal combustion), manufacturing (cement production, electronics, and gold), waste recovery, and recycling.[1]

Recently, we demonstrated that supported chlorocuprate(II) ionic liquids were highly effective at capturing mercury from gases.[2] These supported ionic liquids have been successfully deployed in commercial scale mercury removal units in the oil and gas industry.[3,4] From our initial investigation, we proposed[2] that elemental mercury was trapped within the ionic liquid as a result of two-electron oxidation by chlorocuprate(II) anions, generating chloromercurate(II) species that were integrated as components of a new composite ionic liquid, following the scheme (with $\chi_{CuCl_2} = 0.5$ in the ionic liquid[5]):

$$Hg(0) + [Cu_2Cl_6]^{2-} \longrightarrow [HgCl_3]^- + [CuCl_2]^- + CuCl$$

This mechanism was based on the observation that the reactive dissolution of liquid mercury in bulk chlorocuprate(II) ionic liquids gave solutions with a single ^{199}Hg NMR signal shifted downfield by *ca.* 400 ppm relative to $HgCl_2$, which was consistent with spec-

[a] *The Diamond Light Source, Harwell Science & Innovation Campus, Didcot, Oxfordshire, OX11 0DE*

[b] *QUILL, School of Chemistry and Chemical Engineering, The Queen's University of Belfast, Belfast, BT9 5AG, Northern Ireland. Tel: +44 (0) 28 9097 4836; E-mail: j.holbrey@qub.ac.uk*

[c] *Current address; School of Chemical Engineering and Analytical Science, The University of Manchester, Oxford Road, Manchester, M13 9PL*

† Electronic Supplementary Information (ESI) available: EXAFS of mercury standards, MCA fluorescence data capture times, Hg L_3-edge XANES and IPD data from Hg captured by the supported ionic liquid. See DOI: 10.1039/b000000x/

tra obtained from the corresponding chloromercurate(II) ionic liquids. In addition, while screening supported chlorocuprate(II) ionic liquids for mercury vapour capture, the quantity of mercury captured at the breakthrough point consistently approached half the molar copper content in the fixed-bed.[2]

The binding and speciation on mercury on many conventional adsorbents has been studied using X-ray absorption spectroscopy (XAS).[6–11] Oxidation states, speciation and the formation of mercury oxide, chlorides or sulfides have been directly determined by combining X-ray Absorption Near Edge Structure (XANES) and Extended X-ray Absorption Fine Structure (EXAFS). However, despite the growing application of *in situ* XAS methods to the study of catalytic processes[12–16] providing information under flow conditions, studies of mercury adsorbents have been confined to pre-treated, static samples.

We report here the first *operando* study of mercury capture in a supported ionic liquid adsorbent, using time and spatially resolved XANES and EXAFS spectroscopy. We confirm that mercury is initially captured by the supported ionic liquid *via* two electron oxidation, forming mercury(II) chloride species within the ionic liquid. Moreover, we report a subsequent, slower comproportionation reaction with additional mercury vapour, leading to formation of mercury(I) chloride species with a Hg−Hg bond. The ramification of this secondary mercury capture mechanism to enhance the efficiency of these supported ionic liquids as mercury scrubbers through the careful selection of operation conditions is discussed.

Experimental

EXAFS measurements on the room temperature ionic liquid 1-octyl-3-methylimidazolium chloride/mercury(II)chloride, $[C_8mim]Cl/HgCl_2$ at $\chi_{HgCl_2} = 0.25$, 0.33 and 0.50, and on mercury(II) oxide (HgO), mercury(I) chloride (Hg_2Cl_2), and mercury(II) chloride ($HgCl_2$) standards were carried out at the Diamond Light Source (I20 beamline) at the Hg L_3 absorption edge using a double crystal Si(111) monochromator with data measured with ion chamber detectors in transmission mode. Samples were mounted in a flat PEEK sample holder, using a Teflon spacer with thickness of 100 μm sandwiched between two Kapton foil windows. Three to five spectra were recorded and were then summed, calibrated, and background subtracted using Athena.[17] The spectra were then fitted using Artemis[17] to calculate interatomic distances and their root-mean-square variations (σ^2).

Operando mercury capture was conducted in a continuous flow mode using a small-scale supported ionic liquid capture bed incorporating a PSA 10.534 Cavkit Mercury generator and Sir Galahad II in-line mercury analyser, mounted on the B18 XAS beamline at the Diamond Light Source, Harwell, U.K. The optical line was set up in step scan mode mode with a fast scanning Si(111) double crystal monochromator. EXAFS data were collected in both transmission and fluorescence modes. Fluorescent data were recorded using a high rate fluorescence 36-element Ge detector, and transmission mode data were obtained using an ionisation chamber detector.

The solid-supported ionic liquid, containing 10 wt% of 1-butyl-3-methylimidazolium hexachlorodicuprate(II) ($[C_4mim]_2[Cu_2Cl_6]$) impregnated on porous silica, was prepared as previously reported.[2] Elemental and ICP analysis of the supported ionic liquid gave copper and chloride contents of 2.0% and 3.3% (w/w), respectively, consistent with 10 wt% loading of $[C_4mim]_2[Cu_2Cl_6]$. 60 mg of the sieved adsorbent was loaded as a short packed bed into the 3 mm i.d. quartz tube, producing a bed length of approximately 2 cm. This was mounted horizontally in the beam-line, positioned at 45° to the X-ray beam to facilitate collection of both transmission and fluorescence spectra (Figure 1).

The bed inlet was connected to a Hg vapour generator and the outlet gas from the adsorbent bed to the mercury analyser to enable continuous monitoring of the concentration of mercury leaving the reactor. As far as possible, the experimental set-up replicated the lab-scale test rig previously described[2] for accelerated breakthrough testing with inlet mercury concentration of 2000 ng dm^3 in N_2. The key difference was that the gas flow rate used was lower (190 cm^3 min^{-1} compared to 500 cm^3 min^{-1}) due to experimental limitations. This increased the gas residence time on the adsorbent from *ca.* 8-16 ms previously to *ca.* 50 ms. Under these experimental conditions, the estimated life-time of the adsorbent bed was 150 h.

Once the experimental configuration was in place, and having established that there was gas flow through the bed (using mercury-free carrier gas feed), the mercury capture experiment was started. Data were collected controlled by a program that sequentially placed the focussed X-ray beam at five defined positions down the bed (position 1 was as near to the top edge as possible, followed by position 2 sited 1 mm further down the bed and then positions 2–5 respectively at 2 mm, 3 mm and 4.5 mm from position 1) and then returned to position 1 and repeated the cycle. At each position, the X-ray absorption spectra, Cu K-edge (8.984 eV) and Hg L_3-edge (12.284 eV) EXAFS data were collected in both transmission and fluorescence modes. Five spectra were collected on each edge, each taken for 3 minutes, at each of the five points in the sample that had been selected.

L_3-edge (12.284 eV) EXAFS data were processed using Athena.[17] The XANES region was analysed to determine the inflection point difference (IPD)[7] from the first and second derivatives of absorption coefficient μ(E). These vary with the oxidation state of the mercury sites and its environment, and can be used to identify mercury species (typical values for standard mercury samples are shown in Table S1†). Qualitative analysis of the EXAFS spectral region was made by comparison of the radial structure functions (RSFs) with those of the mercury-containing standards above. For the Hg L_3-edge, fluorescence data gave a better signal-to-noise ratio while for the Cu K-edge, the transmission mode data was of better quality. Only the mercury EXAFS data is shown here.

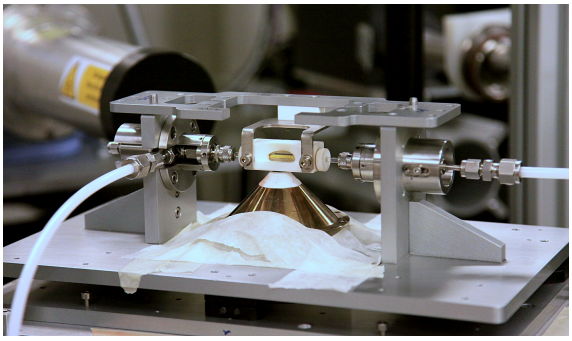

Fig. 1 The adsorbent bed, in place on the B18 EXAFS beamline at Diamond. The stage was moved in 1 mm steps to enable data collection at five positions along the adsorbent bed.

Table 1 EXAFS fits for chloromercurate(II) coordination in the neat room temperature $[C_8mim]Cl/HgCl_2$ ionic liquids at different Hg:Cl ratios.

χ_{HgCl_2}	Coordination number /N	σ^{2a}	R-factor	d /Å
0.50	3	0.00907	0.01723	2.38
0.33	4[b]	0.00705	0.00480	2.48
0.25	4[b]	0.00702	0.00509	2.48

[a] Mean-square disorder in R (Debye-Waller factor), [b] refined to tetrahedral geometry.

Results and Discussion

Mercury coordination in $[C_8mim]Cl/HgCl_2$ ionic liquids

Mercury coordination in the model chloromercurate(II) ionic liquids, $[C_8mim]Cl/HgCl_2$ at $\chi_{HgCl_2} = 0.25$, 0.33 and 0.50 was determined using EXAFS on beamline I20 at Diamond. EXAFS data and the corresponding *pseudo*-radial distribution functions (PRDFs) are shown in Fig. 3. At each composition, a single peak is observed in the PRDFs at around 2.0 Å. The PRDFs provide structural information about the bonding distance between the absorbing (*i.e.* mercury) atom and neighbouring atoms, and it is worth noting that the real bond distances between an absorbing atom and a coordination shell are usually larger than the peak positions in the PRDF due to the scattering phase shift,[18] typically by around 0.5 Å. This single peak at *ca.* 2.0 Å is at a distance consistent with the first coordination sphere of mercury containing exclusively chlorine atoms in a symmetric environment.

The mercury environments in the ionic liquid anions were refined, initially fixing the number of chlorine atoms (N) at 3 for $\chi_{HgCl_2} = 0.50$ and to 4 for $\chi_{HgCl_2} = 0.33$ or 0.25. Good fits to the experimental EXAFS data, shown in Figure 3, indicate the presence of monometallic trigonal-planar $[HgCl_3]^-$ anions at $\chi_{HgCl_2} = 0.50$ and the formation of tetrahedral $[HgCl_4]^{2-}$ anions (Figure 2) in the presence of excess chlorine ($\chi_{HgCl_2} \leq 0.33$). The alternative square planar geometry for $[HgCl_4]^{2-}$ was considered to be unlikely in the ionic liquid on the basis of the comparable ^{199}Hg NMR chemical shifts from the ionic liquids

$[P_{66614}]_2[HgCl_4]$[19] and $[C_4mim]_2[HgCl_4]$[2] to solution state tetrahedral tetrachloromercurate(II) anions.[20]

Fitting EXAFS data from $[C_8mim]Cl/HgCl_3$ $\chi_{HgCl_2} \leq 0.33$ system using a square planar chloromercurate geometry taken from the crystal structure of $K_2[HgCl_4]\cdot H_2O$[21] gave a poorer fit of the model to the data (R factor = 0.0143) compared to that from the tetrahedral configuration in Table 1. Moreover, the Debye-Waller factor (σ^2) for Cl was extremely large (0.083), an order of magnitude larger than for the corresponding tetrahedral fit, suggesting that the chlorine atoms are significantly displaced from a square planar arrangement around mercury. In addition, the absence of multiple scattering interactions along Cl−Hg−Cl pathways that would only be observed in a square planar system also support this conclusion.

Mixed coordination numbers between 3 and 4 were also considered allowing N to vary, and in each case the data refined to integer values of $N = 3$ and 4 respectively.

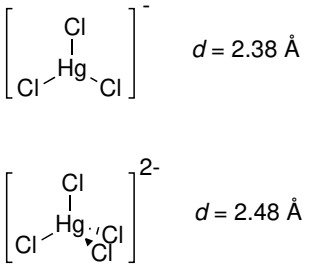

Fig. 2 Geometries, and the calculated Hg–Cl bond length (d), for the trigonal $[HgCl_3]^-$ and tetrahedral $[HgCl_4]^{2-}$ anions identified in the 1-octyl-3-methylimidazolium chloromercurate(II) ionic liquids at χ_{HgCl_2} = 0.33 and 0.50 respectively.

For each ionic liquid composition, the Hg-Cl bond length (Table 1) is slightly longer than that reported for $HgCl_2$ in either aqueous or dimethylsulfoxide solutions (2.29(2) and 2.31(2) Å, respectively).[22] A small, anticipated elongation of the bond, from 2.38(0) to 2.48(2) Å, is observed as the mercury coordination number increases from three, $[HgCl_3]^-$, to four, $[HgCl_4]^{2-}$.

Comparable PRDFs for HgO and $HgCl_2$ also feature a single distinctive first shell peak (Figure S1)†. For HgO, this is centred at 1.67 Å for the short Hg−O bond (2.05 Å), whereas in $HgCl_2$, the longer Hg−Cl bond distance of 2.28 Å gives rise to the peak in the PRDF at 1.87 Å. In contrast, two peaks are observed in the PRDF of Hg_2Cl_2 at 2.04 Å and 2.46 Å from the Hg−Cl bond (2.53Å) and the longer Hg−Hg bond (3.21 Å) characteristic of Hg(I) compounds.[10,23] Peak positions and the corresponding bond lengths for these mercury standards and the two chloromercurate(II) ionic liquids are given in Table 2.

The absence of peaks attributable to Hg···Hg correlations (around 2.8 Å) and the electron density consistent with three chlorine atoms in the first coordination shell around mercury show that, even in the high χ régime, the ionic liquids contain monomeric chloromer-

Table 2 Positions of first shell peak in the Hg L_3 EXAFS PRDFs of reference compounds and the two ionic liquid chloromercurate(II) species.

Material	First peak in PRDF /Å	*d* /Å	*lit.* /Å
HgO	1.67	2.05	2.05[10,23]
$HgCl_2$	1.87	2.29	2.28[10,23]
Hg_2Cl_2	2.04[a]	2.55	2.53[10,23]
$[HgCl_3]^-$	1.95	2.38	
$[HgCl_4]^{2-}$	2.06	2.48	

[a] Second peak at 2.45 Å from Hg−Hg (bond distance 3.21 Å)

curate(II) anions, *i.e.* $[HgCl_3]^-$ rather than oligomeric ones, for example $[Hg_2Cl_6]^{2-}$. Such dimeric anions have been observed in the crystal structures of some imidazolium halomercurate(II) salts[24] and have been proposed as components of ionic liquid based on ^{199}Hg NMR spectroscopy.[19]

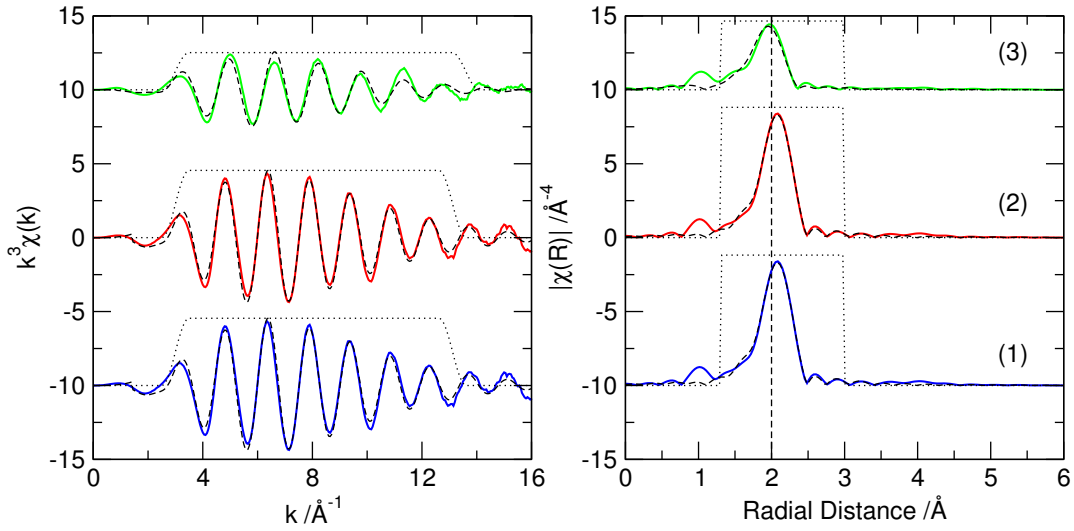

Fig. 3 k^3-Weighted mercury L_3-edge fluorescence EXAFS and corresponding *pseudo*-radial distribution functions (solid lines) and fits (dashed lines) from neat $[C_8mim]Cl/HgCl_2$ ionic liquids at χ_{HgCl_2} = 0.25 (1), 0.33 (2), and 0.50 (3) showing a single peak in the first coordination shell around 2.0 Å.

Operando examination of supported ionic liquid adsorbent

For the *operando* study of mercury capture, the nitrogen carrier gas containing 2000 ng dm^3 of elemental mercury vapour was passed through the supported ionic liquid adsorbent column (60 mg, 0.3 × 20 mm) with a flow rate of 190 cm^3 min^{-1}. XAS (fluorescence, Cu and Hg EXAFS) data were collected sequentially at five positions along the bed, scanning

approximately the first 5.5 mm of the supported ionic liquid. Cu EXAFS were collected first in both fluorescence and transmission modes at each position (5×3 min.) followed by Hg EXAFS (5×3 min) resulting in data sets collected on each edge at each position approximately every 3 h (Table S2)†.

A total gas volume of 205 litres containing 0.41 mg of mercury was treated, with the outlet mercury concentration remaining constantly lower than 0.1 ng dm^{-3} throughout the measurement period, *i.e.* mercury scrubbing was >99.995% efficient.

Absorbance

Capture of mercury as a function of time was followed by examining the relative intensities of the signals from Hg $L_{\alpha 1}$ and Cu $K_{\alpha 1}$ bands around 10 and 8 keV, respectively, using the MCA data generated by the multi-element fluorescence detector, at the five defined positions along the adsorbent bed.

Over the duration of the experiment, at each time and position for which an absorption spectrum was taken (Table S2)†, the bands due to copper remained at constant intensity, indicating a stable distribution of ionic liquid within the support with no displacement in response to the gas flow. In contrast, and as anticipated, the signals arising from mercury captured by the bed increased with time on-line. At the start of the experiment, Hg $L_{\alpha 1}$ signals were not detectable at any point along the bed. After 3 h, small Hg $L_{\alpha 1}$ absorption bands could be observed at the first three positions, whilst at positions 4 and 5, the responses remained indistinguishable from the baseline (Fig. 4). At each position, once a Hg $L_{\alpha 1}$ signal had been detected, the intensity (corresponding to concentration of mercury present) of the band increased over time as more mercury was passed through, and captured on, the bed. The detector response was calibrated by summing the Hg $L_{\alpha 1}$ absorption bands at each position at $t = 6$ h, normalised to the total mercury vapour captured at this point (136.8 μg). This enabled the time and space resolved mercury absorption to be mapped (Fig. 5) and shows the efficient mercury capture at the front of the bed, with progressive movement of a relatively broad adsorption front along the bed as the experiment progressed.

It was estimated that the top 25 % of the adsorbent bed (*i.e.* the positions monitored) would saturate after *ca.* 50 h, therefore over the time-scale of the measurements here, we anticipated a continuous increase in the mercury concentration at all positions without saturation. Indeed, the total mercury captured (summed across the positions screened) increased linearly ($y = 30.618x - 41.115, R^2 = 0.9999$) over the first 15 h, followed by a small deviation as the mercury front moves further down the packed bed. It is worth noting that at positions 4 and 5, mercury could not be detected until after $t = 6$ h at position 4 (Fig. 4).

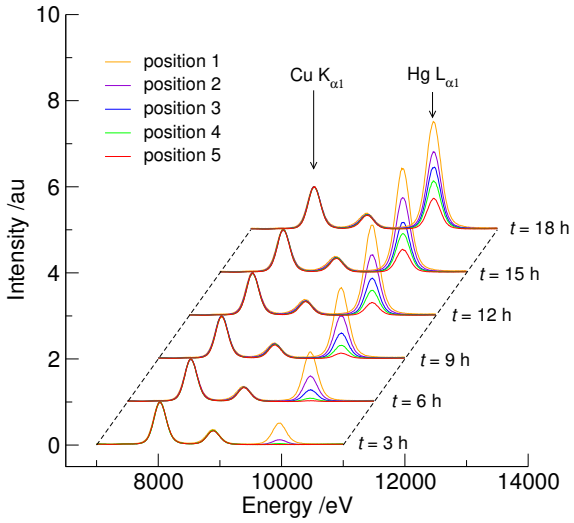

Fig. 4 Stacked plot showing X-ray absorption spectra at each position sampled down the bed at times t = 3, 6, 8, 12, 15 and 18 h, showing the presence, and increase, in mercury captured from the change in the size of the Hg $L_{\alpha1}$ band at 10 keV compared to the constant intensities of the Cu $K_{\alpha1}$ bands at *ca.* 8 and 8.9 keV from the ionic liquid on the bed. Each time-set of fluorescence spectra are offset by 500 eV and by 1 unit in intensity from the previous sets to aid clarity.

XANES

In many cases, XANES can be used to determine the oxidation state and relative electronegativity of the coordination environment of mercury species. Elemental mercury is readily distinguishable from oxidised forms, and oxo- and chloro-coordination environments can be differentiated from the inflection point difference (IPD), taken from the separation of the two peaks in the first derivative spectra of the edge jump. These peaks are associated with inflection points on the excitation edge and the magnitude of the IPD reflects the ionicity of the bonds, with more ionic compounds having larger IPD values whereas more covalent mercury compounds give rise to smaller values.[7,10] Data for the mercury standards, HgO, $HgCl_2$, Hg_2Cl_2 and for the ionic liquid $[C_8mim][HgCl_3]$ are shown in Figure S1 and Table S1†.

An edge jump for mercury could not be detected at the start of the experiment. After running the mercury-containing gas through the bed for 3 h, a small Hg L_3 edge jump (with poor signal-to-noise resolution) could be observed in the fluorescence X-ray absorption spectra (see Figure S2). This was consistent with the onset of detection of Hg L-bands in Figure 4, and similar responses were observed at the remaining positions along the bed, with the signal-to-noise ratio improving incrementally with time at each position.

Hg L_3-edge XANES spectra were examined at each position/time combination where an edge jump could be detected and were compared to the reference materials. All mercury XANES spectra from the absorption bed show multiple shoulders, and are therefore inconsistent with the presence of physisorbed elemental mercury. This indicates that the

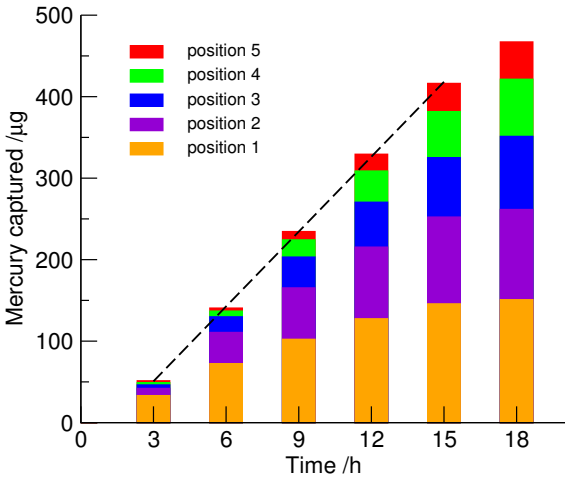

Fig. 5 Total mercury captured on the adsorbent bed plotted as a function of time and subdivided into the concentrations at each position along the bed.

mercury detected in the adsorbent is not capillary condensed metallic mercury. Two peaks were found in the Hg L_3-edge XANES first derivative spectral plot with an IPD in the range 8.2–8.7 eV in each data set (shown in Figure S3 and Table S3).†These values all fall within the experimental range of both Hg(I) and Hg(II) in chloride-rich environments, including the two chloromercurate(II) ionic liquids, and are significantly smaller than the IPD for HgO (*ca.* 14 eV). This establishes that mercury is captured in the supported ionic liquid bed as a chloro-complex, but provides no further quantitative structure identification.

EXAFS

In contrast to the XANES, *pseudo*-radial distribution functions calculated from the EXAFS data show differences between the molecular mercury chlorides ($HgCl_2$ and Hg_2Cl_2) and the chloromercurate(II) ionic liquids (Fig. 3). This provides a means to characterise the coordination and speciation of mercury captured in the supported ionic liquid (Table 2).

Hg L_3-edge EXAFS spectra were obtained at all the sample positions and collection times for which a signal was detectable in the XFS spectra, with a limiting sensitivity to detection of approximately 35 ng Hg. Unsurprisingly, when the edge jump was small due to low concentrations of mercury present, the signal-to-noise ratio in the data was poor, but improved with time online.

The k^3-weighted Hg L_3-edge EXAFS from position 1 of the adsorbent bed (near the bed front) are shown in Fig. 6. Similar results were observed at all the positions along the bed, with corresponding time delays before detection of the mercury EXAFS PRDF. In the data collected at $t = 2.5$ h, the predominant feature observed is the large single peak at 1.96 Å, which resembles that of $[C_8mim]Cl/HgCl_2$ ($\chi_{HgCl_2} = 0.50$) ionic liquid with a three coordinate $[HgCl_3]^-$ anion (PRDF peak position 1.95 Å). This appears to support the initial proposal that mercury is captured by the supported ionic liquid *via* oxidation and leads to

the formation of chloromercurate(II) anions. The more chloride-deficient $[HgCl_3]^-$ anion is initially formed rather than $[HgCl_4]^{2-}$.

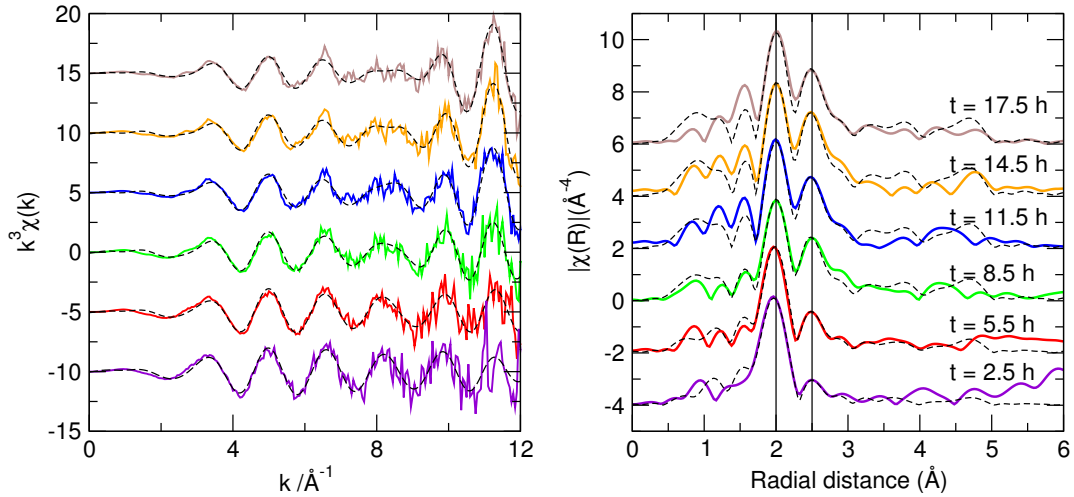

Fig. 6 k^3-Weighted mercury L_3-edge fluorescence EXAFS and corresponding *pseudo*-radial distribution functions (solid lines) and best fits (dashed lines) for the supported ionic liquid at position 1 of the adsorbent bed plotted at 3 h time intervals, showing the shift from a single peak in the correlation shell around 2.0 Å and the emergence of a second peak which grows in intensity at 2.5 Å.

A small peak centred at 2.5 Å also appears to be present in the data. Considered in isolation, this signal is of the same magnitude as the noise in the spectrum (which is large due to the low concentrations of mercury present and the associated small edge jump obtained). However, comparing how the spectra in Fig. 6 evolve, the signal at 2.5 Å grows over time and represents the formation of a measurable structural feature. In addition, the position of the first peak in the PRDF around 2.0 Å, associated with Hg−Cl bonds, extends slightly to *ca.* 2.05 Å by $t = 17.5$ h. The presence of the second peak at 2.5 Å suggests a mercury–mercury correlation. By comparison with the EXAFS data for mercury(I) and mercury(II) chlorides, the most likely candidate is mercury(I) chloride, *e.g.* calomel (Hg_2Cl_2), which is characterised by the presence of a short Hg–Hg bond. Indeed, the EXAFS spectrum at $t = 17.5$ h (in Fig. 6) closely resembles that of mercury(I) chloride, Hg_2Cl_2, with both Hg−Cl and Hg−Hg coordination to the central mercury site.

Linear combination analysis (LCA) of the Hg-edge EXAFS data (combining experimental sets from $[C_8mim][HgCl_3]$ and $[Hg_2Cl_2]$) was used to determine the fraction of Hg(II) and Hg(I) present at position 1 in the bed as a function of time. The results (Fig 7) show that initially at $t = 3$ h, *ca.* 90% of the mercury captured is present as Hg(II) and *ca.* 10% as Hg(I). However, as the time on-line increases, the Hg(I) component rises to *ca.* 70% after 15 h.

These results indicate that mercury is initially captured by the ionic liquid through an

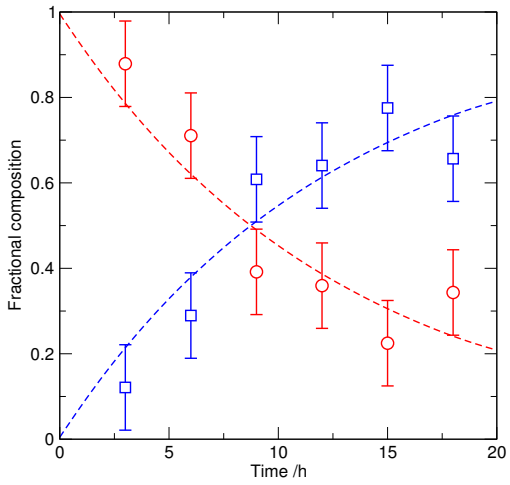

Fig. 7 Ratio of Hg(I):Hg(II) present at position 1 on the supported ionic liquid adsorbent bed, calculated by determined by linear correlation analysis of the XAFS PRDF as a function of time, showing the conversion of captured mercury from Hg(II) (red circles) to Hg(I) (blue squares).

oxidative process, forming $[HgCl_3]^-$ chloromercurate(II) anions, analogous to those in the neat ionic liquid. These Hg(II)-containing anions are then subsequently transformed to Hg(I)-chloride species. One plausible explanation is comproportionation through reaction of gaseous elemental Hg(0) with the $[HgCl_3]^-$ anions within the supported ionic liquid once the local oxidising Cu(II) rich environment is consumed, although the potential for photoreduction induced by the X-ray beam itself cannot be excluded.

X-ray induced photoreduction has been observed during XPS and XAS experiments using high energy synchrotron radiation sources with a number of different metals in a wide range of environments.[25] Mercury(II) photoreduction during EXAFS measurements of Hg(II) adsorbed onto γ-alumina has been proposed.[8] In contrast, Li *et al.*[10] reported that they did not observe either formation of Hg(I) or any X-ray induced photoreduction during XANES and EXAFS spectroscopy studies of mercury adsorption by copper chloride impregnated activated carbons. Instead, and as we originally anticipated *in this work*, the formation of Hg-Cl bonds was observed with the conclusion that $HgCl_2$ was the most likely product formed. In common with the procedure we previously used for accelerated break-through screening, Li *et al.* loaded mercury onto small adsorbent samples (100 mg) using a carrier gas with a high inlet Hg(0) concentration (3000 ng dm^{-3}) and high gas flow rates (500 cm^3 min^{-1}) to achieve equilibrium capacities prior to XAS measurements.

Hg(0) capture by chloromercurate(II) ionic liquids

Comproportionation, with a net one-electron oxidative scrubbing of mercury from the vapour phase, would be the simplest explanation for the formation of Hg(I), providing a secondary mechanism for Hg(0) capture:

$$Hg + [HgCl_3]^- \longrightarrow Hg_2Cl_2 + Cl^-$$

This could extend the design-life of solid supported ionic liquids used in mercury removal units.

In order to test whether the comproportionation mechanism is feasible to explain formation of Hg(I) in the EXAFS experiments, accelerated breakthrough testing for gas phase mercury capture was performed using a solid supported 1-butyl-3-methylimidazolium trichloromercurate(II) ([C_4mim][$HgCl_3$]) ionic liquid as adsorbent. Experimental conditions reproduced those previously described,[2] using supported chloromercurate(II) ionic liquids, and the carrier gas flow rate was varied. Fig. 8 shows the outlet mercury concentration profiles obtained as a function of time testing at two different has flow rates, 190 cm^3 min^{-1} (**2**) and 484 cm^3 min^{-1} (**1**).

At 190 cm^3 min^{-1}, corresponding to the flow rate used for the XAS measurements above, mercury capture was observed by the supported [C_4mim][$HgCl_3$] ionic liquid with the $[Hg]_{out}$ initially reduced to 0.1 ng dm^{-3} from an inlet concentration of 2000 ng dm^{-3}. This efficient scrubbing was maintained for 2 h, and was then followed by a slow increase in $[Hg]_{out}$ reaching 2 ng dm^{-3} after 5.5 h. Measurement was halted at this point as the objective, to demonstrate that a supported chlorometallate(II) ionic liquid could capture mercury, had been achieved. It should be noted that reducing $[Hg]_{out}$ = 2 ng dm^{-3} corresponds to capture of 99.9 % of the input mercury.

Under higher flow conditions, (**2**, in Fig. 8), which replicates the contact times on the adsorbent beds used in our previous work with $[C_4mim]_2[Cu_2Cl_6]$,[2] $[Hg]_{out}$ was initially reduced to < 5 ng dm^{-3}. However, after 30 min the outlet mercury concentration started to rise and after 1 h had exceeded 20 ng dm^{-3}. Control experiments using silica impregnated with the metal-free ionic liquid, [C_4mim]Cl, as an adsorbent showed no mercury adsorption (not shown). This result is consistent with recent studies that report poor capture of elemental mercury by imidazolium halide ionic liquids (in the order of, at best, a few tens of mg per g of ionic liquid)[26,27] unless an oxidant is present.[27,28]

These results demonstrate that chloromercurate(II) ionic liquids can function as adsorbents to capture additional mercury gas, with the most credible mechanism being comproportionation of Hg(II) and Hg(0). This is supported by the generation of Hg(I) species observed in the *operando* EXAFS studies.

Mercury capture by the supported chlorocuprate(II) ionic liquid is efficient under high flow (low contact time) conditions which is indicative of rapid reaction of mercury with the ionic liquid. As previously reported,[2] with a gas flow rate of 600 cm^3 min^{-1} (corresponding to a contact times of *ca*. 8-16 ms), complete mercury capture is observed up until breakthrough at the point where the mercury content in the support approaches *ca.* 1:2 Hg:Cu. This suggests a reaction rate that is greater than at least *ca*. 100 s^{-1}, probably significantly so. In contrast, the reaction of mercury vapour with chloromercurate(II) species

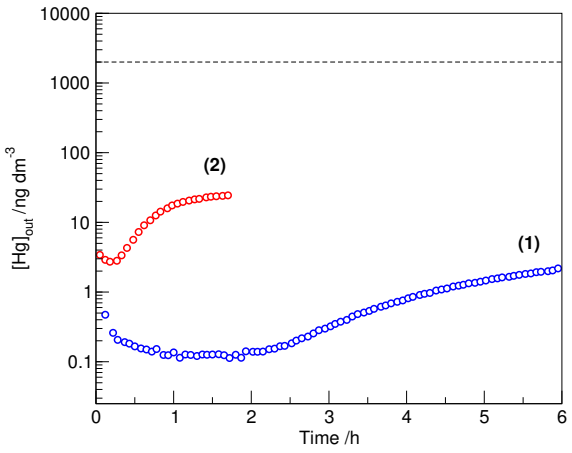

Fig. 8 Mercury outlet concentrations from capture of mercury vapour from nitrogen carrier gas ($[Hg]_{in}$ = 2000 ng dm^{-3}, T = 25 °C) using 10 wt% $[C_4mim][HgCl_3]$ on porous silica (surface area; 135 m^2 g^{-1}, pore volume; 0.83 cm^3 g^{-1}) at (**1**) 190 cm^3 min^{-1} and (**2**) 484 cm^3 min^{-1}. The upper horizontal dashed line indicates the inlet mercury concentration (2000 ng dm^{-3}).

is much slower, as can be seen from the sensitivity of the $[Hg]_{out}$ profile to the gas flow rate (and corresponding differences in vapour-adsorbent contact times) in Figure 8.

These differences in reaction rates (although not quantifiable based on the data available here) for the two sequential reactions; mercury(0) with copper(II), and mercury(0) with mercury(II) rationalise why efficient capture corresponding to a two-electron oxidative process was previously obtained[2] with short contact times, whereas using a slower flow rate and correspondingly longer contact time, comproportionation of Hg(0) with Hg(II) provides a secondary reaction pathway that can lead to overall one-electron oxidative capture.

In typical mercury removal units designed for gas treatment, gas contact times of 5–20 s are usual.[29] Under these operating conditions it is highly likely that both chlorometallate(II) species will play active roles in Hg(0) capture. This will allow net one-electron oxidative capture of mercury by the supported ionic liquid, effectively doubling the design capacity of chlorocuprate(II)-based ionic liquid mercury adsorbents.

Conclusions

An *operando* EXAFS study of the capture of mercury from the gas phase by a supported $[C_4mim]_2[Cu_2Cl_6]$ ionic liquid has been performed. Efficient trapping of mercury, initially as a Hg(II)-chloride species, was observed. This was followed by the unanticipated secondary comproportionation reaction with Hg(0), forming Hg(I)-species containing a characteristic Hg–Hg bond identified by the PRDF peak at 2.5 Å from the EXAFS data.

The ability to capture mercury vapour using preprepared supported chloromercurate(II) ionic liquids was also examined in order to establish the feasibility of the comproportionation mechanism (irrespective of any possible beam induced X-ray photoreduction in the

EXAFS measurements). Scrubbing was effective when a contact time around 50 ms was used (with >99.9% mercury removal over the 5.5 h screen). If the contact time was reduced to *ca.* 20 ms (comparable to previous measurements using chlorocuprate(II) ionic liquids), an increase in the mercury content of the outlet gas was seen after only 30 min. This indicates that the reaction of $[HgCl_3]^-$ with Hg(0) is significantly slower than that of $[Cu_2Cl_6]^{2-}$, although kinetics were not explicitly studied here.

Acknowledgements

We acknowledge PS Analytical (Orpington, Kent, UK,) for the generous loan and installation of the Cavkit and Sir Galahad mercury generator and detector on the Diamond beamline, the Diamond Light Source for time on beam lines I20 and B18 under proposals SP2452 and SP11881, and to PETRONAS for funding a PDRA fellowship (GS) and studentship (RR).

References

1 (*a*) S. Liang, Y. Wang, S. Cinnirella and N. Pirrone, *Env. Sci. Technol.*, 2015, **49**, 3566–3574; (*b*) K. J. Lee and T. G. Lee, *J. Hazard. Mater.*, 2012, **241-242**, 1–13.

2 M. Abai, M. P. Atkins, A. Hassan, J. D. Holbrey, Y. Kuah, P. Nockemann, A. A. Oliferenko, N. V. Plechkova, S. Rafeen, A. A. Rahman, R. Ramli, S. M. Shariff, K. R. Seddon, G. Srinivasan and Y. Zou, *Dalton Trans.*, 2015, **44**, 8617–8624.

3 M. Abai, M. Atkins, K. Cheun, J. Holbrey, P. Nockemann, K. Seddon, G. Srinivasan and Y. Zou, *Process for removing metals from hydrocarbons*, 2012, WO Patent App. PCT/GB2011/051906.

4 *Clariant and PETRONAS sign licensing collaboration, http://newsroom.clariant.com/clariant-and-petronas-sign-licensing-collaboration*, 2014.

5 J. Estager, J. D. Holbrey and M. Swadźba-Kwaśny, *Chem. Soc. Rev.*, 2014, **43**, 847–886.

6 F. E. Huggins, G. P. Huffman, G. E. Dunham and C. L. Senior, *Energy Fuels*, 1999, **13**, 114–121.

7 F. E. Huggins, N. Yap, G. P. Huffman and C. L. Senior, *Fuel Process. Technol.*, 2003, **82**, 167–196.

8 C. Kim, J. Rytuba and G. Brown, *J. Colloid Interface Sci.*, 2004, **271**, 1–15.

9 S. Poulston, T. I. Hyde, H. Hamilton, O. Mathon, C. Prestipino, G. Sankar and A. W. J. Smith, *Phys. Chem. Chem. Phys.*, 2010, **12**, 484–491.

10 X. Li, J.-Y. Lee and S. Heald, *Fuel*, 2012, **93**, 618–624.

11 T. M. Bisson, L. C. W. MacLean, Y. Hu and Z. Xu, *Env. Sci. Technol.*, 2012, **46**, 12186–12193.

12 M. A. Newton, J. B. Brazier, E. M. Barreiro, S. Parry, H. Emmerich, L. A. Adrio, C. J. Mulligan, K. Hellgardt and K. K. M. Hii, *Green Chem.*, 2016, **18**, 406–411.

13 J. B. Brazier, B. N. Nguyen, L. A. Adrio, E. M. Barreiro, W. P. Leong, M. A. Newton, S. J. Figueroa, K. Hellgardt and K. K. M. Hii, *Catal. Today*, 2014, **229**, 95–103.

14 C. Geantet and C. Pichon, in *X-Ray Absorption Spectroscopy*, Wiley-VCH Verlag GmbH & Co. KGaA, 2012, pp. 511–536.
15 R. C. Nelson and J. T. Miller, *Catal. Sci. Technol.*, 2012, **2**, 461–470.
16 C. Lamberti, S. Bordiga, F. Bonino, C. Prestipino, G. Berlier, L. Capello, F. D'Acapito, F. Xamena and A. Zecchina, *Phys. Chem. Chem. Phys.*, 2003, **5**, 4502–4509.
17 B. Ravel and M. Newville, *J. Synchrotron Rad.*, 2005, **12**, 537–541.
18 B. K. Teo, *EXAFS: Basic Principles and Data Analysis.*, Springer-Verlag, Berlin, 1986.
19 A. Metlen, B. Mallick, R. W. Murphy, A.-V. Mudring and R. D. Rogers, *Inorg. Chem.*, 2013, **52**, 13997–14009.
20 (*a*) M. S. Bharara, S. Parkin and D. A. Atwood, *Main Group Chemistry*, 2005, **4**, 217–225; (*b*) G. Klose, F. Volke, G. Peinel and G. Knobloch, *Mag. Reson. Chem.*, 1993, **31**, 548–551.
21 J. Itoh, R. Kusaka, Y. Yamagata, R. Kiriyama and H. Ibamoto, *J. Phys. Soc. Jpn.*, 1953, **8**, 293–301.
22 R. Akesson, I. Persson, M. Sandstrom and U. Wahlgren, *Inorg. Chem.*, 1994, **33**, 3715–3723.
23 A. F. Wells, *Structural Inorganic Chemistry*, Clarendon Press, Oxford, 1984.
24 B. Mallick, A. Metlen, M. Nieuwenhuyzen, R. D. Rogers and A.-V. Mudring, *Inorg. Chem.*, 2012, **51**, 193–200.
25 (*a*) M. Gudmundsson, S. Kim, M. Wu, T. Ishida, M. H. Momeni, G. Vaaje-Kolstad, D. Lundberg, A. Royant, J. Staahlberg, V. G. H. Eijsink, G. T. Beckham and M. Sandgren, *J. Biol. Chem.*, 2014, **289**, 18782–18792; (*b*) J. Yi, A. M. Orville, J. M. Skinner, M. J. Skinner and G. B. Richter-Addo, *Biochemistry*, 2010, **49**, 5969–5971; (*c*) F. Champloy, K. Gruber, G. Jogl and C. Kratky, *J. Synchrotron Radiation*, 2000, **7**, 267–273; (*d*) F. Mercier-Bion, R. Drot, J. J. Ehrhardt, J. Lambert, J. Roques and E. Simoni, *Surf. Interface Anal.*, 2011, **43**, 777–783; (*e*) L. Dubois, L. Jacquamet, J. Pecaut and J.-M. Latour, *Chem. Commun.*, 2006, 4521–4523; (*f*) G. P. Halada and C. R. Clayton, *J. Electrochem. Soc.*, 1991, **138**, 2921–27; (*g*) P. Goncalves Ferreira, D. de Ligny, O. Lazzari, A. Jean, O. Cintora Gonzalez and D. R. Neuville, *Chem. Geol.*, 2013, **346**, 106–112; (*h*) Y.-Y. Fong, B. R. Visser, J. R. Gascooke, B. C. C. Cowie, L. Thomsen, G. F. Metha, M. A. Buntine and H. H. Harris, *Langmuir*, 2011, **27**, 8099–8104; (*i*) J. Yang, T. Regier, J. J. Dynes, J. Wang, J. Shi, D. Peak, Y. Zhao, T. Hu, Y. Chen and J. S. Tse, *Anal. Chem.*, 2011, **83**, 7856–62.
26 (*a*) L. Ji, S. W. Thiel and N. G. Pinto, *Ind. Eng. Chem. Res.*, 2008, **47**, 8396–8400; (*b*) T. Abbas, L. K. Chelappan, M. I. A. Mutalib, K. Y. Cheun, S. N. Shah, S. Nazir, A. Hassan, M. B. Abai and E. Khan, *Ind. Eng. Chem. Res.*, 2015, **54**, 12114–12123; (*c*) T. Abbas, G. Gonfa, K. C. Lethesh, M. I. A. Mutalib, M. b. Abai, K. Y. Cheun and E. Khan, *Fuel*, 2016, **177**, 296–303.

27 (*a*) G. Cheng, B. Bai, Q. Zhang and M. Cai, *J. Hazard. Mater.*, 2014, **280**, 767–773; (*b*) G. Cheng, Q. Zhang and B. Bai, *Chem. Eng. J.*, 2014, **252**, 159–165.

28 Z. Barnea, T. Sachs, M. Chidambaram and Y. Sasson, *J. Hazard. Mater.*, 2013, **244**, 495–500.

29 J. C. Enneking and C. B. Summers, *Proceedings, Annual Meeting - Air & Waste Management Association*, 2007, Paper 146.